

TEXAS A&M UNIVERSITY  
Department of Mechanical Engineering

Prof. Xinghang Zhang  
Department of Mechanical Engineering  
Texas A&M University  
College Station, TX 77843-3123  
Tel: (979) 845-2143  
Fax: (979) 862-2418  
Email: [zhangx@tamu.edu](mailto:zhangx@tamu.edu)

April 29, 2009

**Re: TMS graduate student paper contest applicant - Mr. Engang Fu**

To Whom It May Concern:

I am pleased to write this letter to verify that Mr. Engang Fu is one my Ph.D. students at Texas A&M University. Engang has been working with me on radiation damage in nanostructured Cu/V multilayer films since 2006. He did extensive experiments to examine the mechanical properties and microstructural changes in Cu/V nanolayers before and after helium (He) ion irradiations. One of the most challenging tasks is to identify microstructural defects, such as He bubbles and interstitial loops in radiated specimen by using transmission electron microscopy (TEM). Engang has succeeded in using TEM to identify defects and localized lattice expansions. The microscopy studies are very tedious, and yet very challenging. Engang's other original contribution was to interpret and analyze void swelling and radiation induced hardening in nanolayer films. He went through many reference books and theories to identify the correlations between theoretical predictions and experimental results. He has done a remarkable job in putting all these pieces together into a high quality manuscript.

Please feel free contact me should you have any question regarding his application.

Sincerely yours,

A handwritten signature in black ink, appearing to read "Xinghang Zhang".

Xinghang Zhang

# **Interface Enhanced Radiation Tolerance in Cu/V Nanolayers**

**Engang Fu**

**Materials Science and Engineering Program  
Department of Mechanical Engineering  
Texas A&M University, College Station, TX 77843**

**TMS Student Award Program:**

**Outstanding Student Paper Contest:**

**Graduate Contest under the discipline of Materials Science**

**Address:**

Engang Fu

3123 TAMU

Department of Mechanical Engineering

Texas A&M University

College Station, TX 77843, USA

Phone: (979) 845-8390

Fax: (979) 845-3081

Email: [fuengang@tamu.edu](mailto:fuengang@tamu.edu)

Material Advantage Member No. **455885**

# Interface Enhanced Radiation Tolerance in Cu/V Nanolayers

Engang Fu

Materials Science and Engineering Program

Department of Mechanical Engineering

Texas A&M University, College Station, TX 77843

## Abstract

Sputtered Cu/V nanolayers with individual layer thickness,  $h$ , varying from 1 to 200 nm were irradiated by helium (He) ion at room temperature to a peak dose of 6 displacements per atom (dpa). The average helium bubble density decreases significantly with decreasing  $h$ . The magnitude of radiation hardening decreases with decreasing layer thickness, and becomes negligible when  $h$  is 2.5 nm or less. This study indicates that nearly immiscible Cu/V interfaces with the space of a few nm apart can effectively reduce the concentration of radiation induced point defects. Consequently, Cu/V nanolayers possess enhanced radiation tolerance, i.e., reduction of void swelling and suppression of radiation hardening, compared to monolithic Cu or V.

## 1. Introduction

The radiation-induced defects and evolutions of mechanical properties in proton, neutron and ion irradiated metallic materials have been subject of many experimental and theoretical studies [1-3]. Radiation to the metals and alloys leads to atomic displacement damages, such as vacancies, interstitials, and their agglomerations in the form of vacancy clusters, voids and dislocation loops [4]. In fusion reactors, besides the aforementioned displacement damages, a high concentration of He atoms created via  $(n, \alpha)$  or other

transmutation reactions typically leads to a large number of He bubbles in irradiated structural metals [5]. Radiation induced void swelling can cause significant dimensional instability and degrade the mechanical properties in the form of embrittlement. Significant void swelling, ~ 14%, has been observed in neutron irradiated 316L stainless steels [6]. Radiation hardening has been extensively studied in irradiated FCC and BCC monolithic metals, such as Cu and V [7, 8]. The increase of yield strength is approximately 200-300 MPa in Cu and V irradiated at a damage level of ~ 1 dpa [9].

Microstructural control is an effective way to suppress radiation damage. The aforementioned studies have shown that grain or phase boundaries may act as sinks for radiation induced point defects and their clusters, where recombination of interstitial and vacancy could occur and such recovery process assists the interfaces in maintaining their ability to continuously absorb point defects [10-11]. Metallic nanolayer films possess very high ratio of interfacial area to volume. Recent studies show that immiscible Cu/Nb nanolayers with a layer thickness of a few nm are extremely resistant against He ion irradiation-induced intermixing [12]. Atomistic simulations show that pairs of extended jogs formed by misfit dislocations along interfaces can effectively lower the point defect formation energy, and such interfaces become virtually inexhaustible sinks for point defects and catalysts for efficient Frenkel pair recombination [13].

In this article, we provide a systematic study of He ion irradiation induced defects, void swelling, and the evolution of film hardness in Cu/V nanolayers, and explain the mechanisms that lead to enhanced radiation tolerance in nearly immiscible Cu/V nanolayers.

## 2. Experimental

Cu/V nanolayer films with equal individual layer thickness ranging from 1 to 200 nm were synthesized on Si (100) substrates by using the DC magnetron sputtering technique at room temperature. Details of synthesis method can be found elsewhere [14]. Before helium (He) ion irradiation, the samples with  $5 \times 10$  mm in dimension were partially masked to avoid ion irradiation in the masked regions. After irradiation experiments, the difference in height (step height) between the irradiated and unirradiated regions was measured by using a Dektak 3 Stylus profilometer with a Z height resolution of better than 1 nm. Void swelling is the result of the measured values of step height divided by the ion range ( $\sim 400$  nm) in the current studies. The ion irradiations were performed at room temperature using 50 keV He ions. A total fluence of  $6 \times 10^{20} / \text{m}^2$  was achieved in 4 hours at a constant beam current of 2  $\mu\text{A}$ . Baseline pressure in the ion implanter was less than  $1 \times 10^{-5}$  Pa. The temperature rise of specimens due to beam heating was estimated to be less than 50  $^{\circ}\text{C}$ .

The microstructure of Cu/V nanolayer was examined in a 200 kV JEOL 2010 transmission electron microscope (TEM). The scanning TEM (STEM) and energy dispersive X-ray (EDX) analysis for identifying the elemental composition and the interface integrity of the specimens were performed by the FEI Tecnai F20 with Fischione ultra-high resolution STEM HAADF detector with 0.23 nm resolution and Oxford EDX detector with spatial resolution of  $\sim 1$ -2 nm. The hardness and indentation modulus of films were measured based on an average of 9-12 indents at different indentation depths at room temperature, by a Fischerscope HM2000XYp micro-indenter

using a Vickers indenter with the same loading rate. The maximum indentation depth was kept at  $\sim 200$  nm for all specimens.

### 3. Results

#### 3.1 Microstructural evolutions

Bright field cross-sectional TEM (XTEM) micrographs of the as-deposited and ion irradiated Cu/V 50 nm and Cu/V 2.5 nm nanolayers are compared in Figure 1. The as-deposited Cu/V nanolayers (figure 1a and 1b) possess polycrystalline columnar grain structures with clearly defined layer interfaces and Kurdjumov-Sachs (K-S) orientation relationship: Cu  $\{1\ 1\ 1\}$  // V  $\{1\ 1\ 0\}$  // interface, and Cu  $\langle 1\ 1\ 0 \rangle$  // V  $\langle 1\ 1\ 1 \rangle$ . The columnar grain size in as-deposited Cu/V 50 nm is similar to the individual layer thickness,  $h$ , whereas grain sizes are much greater than  $h$  in the as-deposited Cu/V 2.5 nm specimen. After He ion irradiation, de-focused XTEM experiments were performed to reveal defects induced by He ion irradiation across the entire thickness of the Cu/V 50 nm and Cu/V 2.5 nm specimens, as shown in Fig. 1c and 1d. Superimposed on the images are two depth profiles of He concentration (solid curves starting from surfaces) obtained from SRIM simulations [15] of Cu/V 50 nm and Cu/V 5 nm nanolayer by using experimental radiation parameters. The number of He bubbles in irradiated samples correlates well with the simulated He concentration profile and reaches a maximum at a depth of  $\sim 200$  nm underneath the film surface. SADs in irradiated Cu/V nanolayer samples indicate insignificant change of fiber textures. The magnified XTEM micrographs of the Cu/V 50 nm and Cu/V 2.5 nm specimens at the peak damage regions, as outlined by a square box in Fig. 1c and 1d, are compared in Fig. 1e and 1f. Comparisons of the two micrographs show similar size of He bubbles,  $\sim 1$  nm in diameter

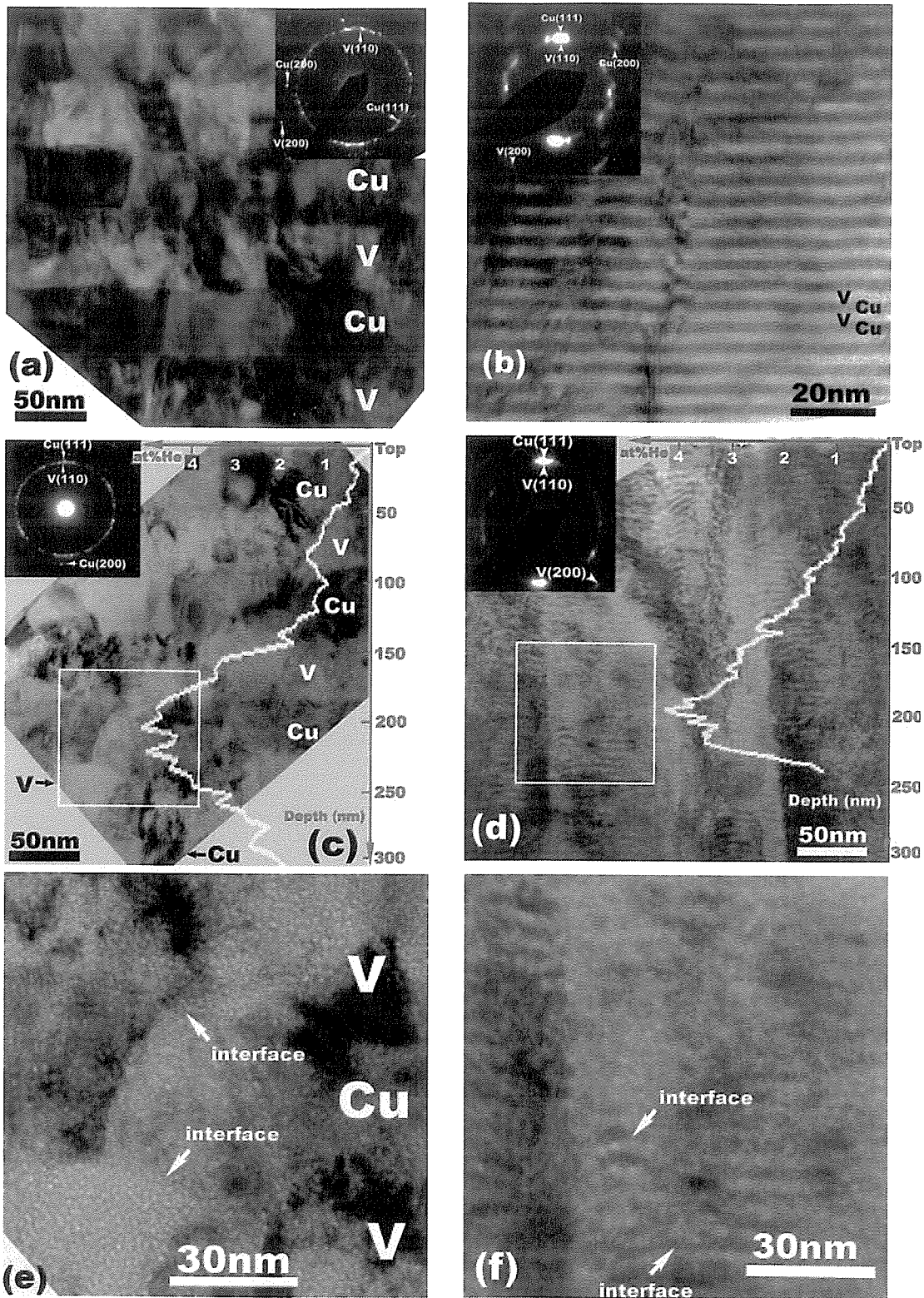
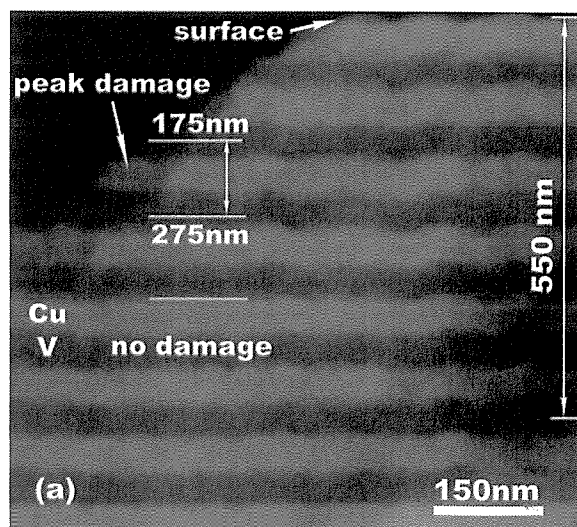


Figure 1, XTEM images of as-deposited (a) Cu/V 50 nm, and (b) Cu/V 2.5 nm nanolayers and He ion irradiated (c) Cu/V 50 nm, and (d) Cu/V 2.5 nm specimens. (e) and (f) are magnified micrographs of the peak damage regions of irradiated Cu/V 50 nm and Cu/V 2.5 nm nanolayers, respectively.

and the density of He bubbles in Cu/V 50 nm specimen is much greater than that of irradiated Cu/V 2.5 nm nanolayers.

STEM experiments were performed to examine the chemical integrity of layer interface after irradiation. A STEM micrograph of ion irradiated Cu/V 50 nm specimen is shown in Fig. 2a. The brighter layers are Cu, sandwiched by the darker V layers. Three different regions predicted by SRIM simulation were examined: (i) a film surface region with low to medium damage, (ii) a peak damage region at a depth of around 200 nm, and (iii) a no damage region that is deeper than the ion projected range. Chemically abrupt layer interfaces are observed in all the three regions. Furthermore, semi-quantitative chemical composition analysis via EDX was performed in the same specimen along a straight line, 550 nm in length, normal to the layer interface across all the regions. As shown in Fig. 2b, the composition profiles for the three regions are essentially the same, indicating that radiation induced interdiffusion across layer interface, if any, is under the spatial resolution limit of such a technique. STEM studies of Cu/V 2.5 nm (not shown here) in the unirradiated and peak damage regions show qualitatively that layer interfaces remain chemically modulated after He ion irradiation.



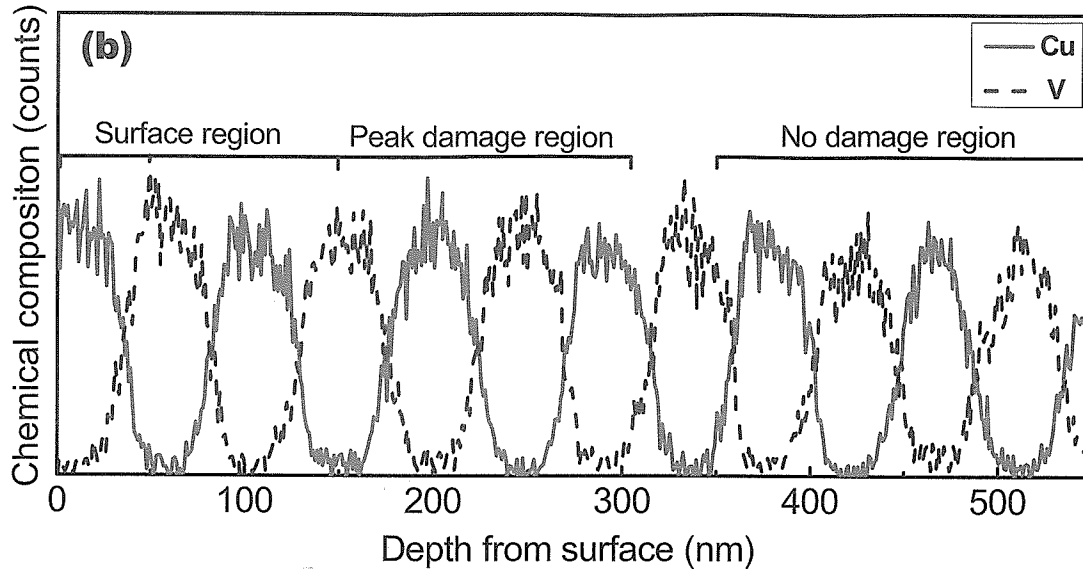


Figure 2, (a) STEM image of ion-irradiated Cu/V 50 nm, and (b) EDX analysis of compositions for the same sample along the straight line, 550 nm in length, normal to the layer interface across all three regions: surface, peak damage, and no damage region.

XTEM was used to examine the influence of individual layer thickness on bubble density in ion irradiated Cu/V nanolayers. Fig. 3a compares the He bubble density as a function of depth from the film surface in irradiated Cu/V 50 nm and Cu/V 2.5 nm nanolayers. He bubble density (number per unit volume) was calculated from TEM micrographs taken at an under-focused condition ( $\sim 400$  nm) where similar bubble sizes ( $\sim 1$  nm) are observed in all irradiated specimens, and sample thickness is assumed to be  $\sim 25$  nm. In both cases, the He bubble density increases rapidly to a maximum at a depth of  $\sim 200$  nm, where the helium concentration reaches a peak according to SRIM simulations. One major difference in the two cases is that the peak He bubble density in the Cu/V 50 nm nanolayer is around 3 times greater than that of Cu/V 2.5 nm specimen. On the other hand, the peak bubble density of irradiated Cu/V 50 nm nanolayer is still lower than that of single layer polycrystalline Cu films, as shown by the horizontal dashed line in Fig. 3a, irradiated at the same condition.

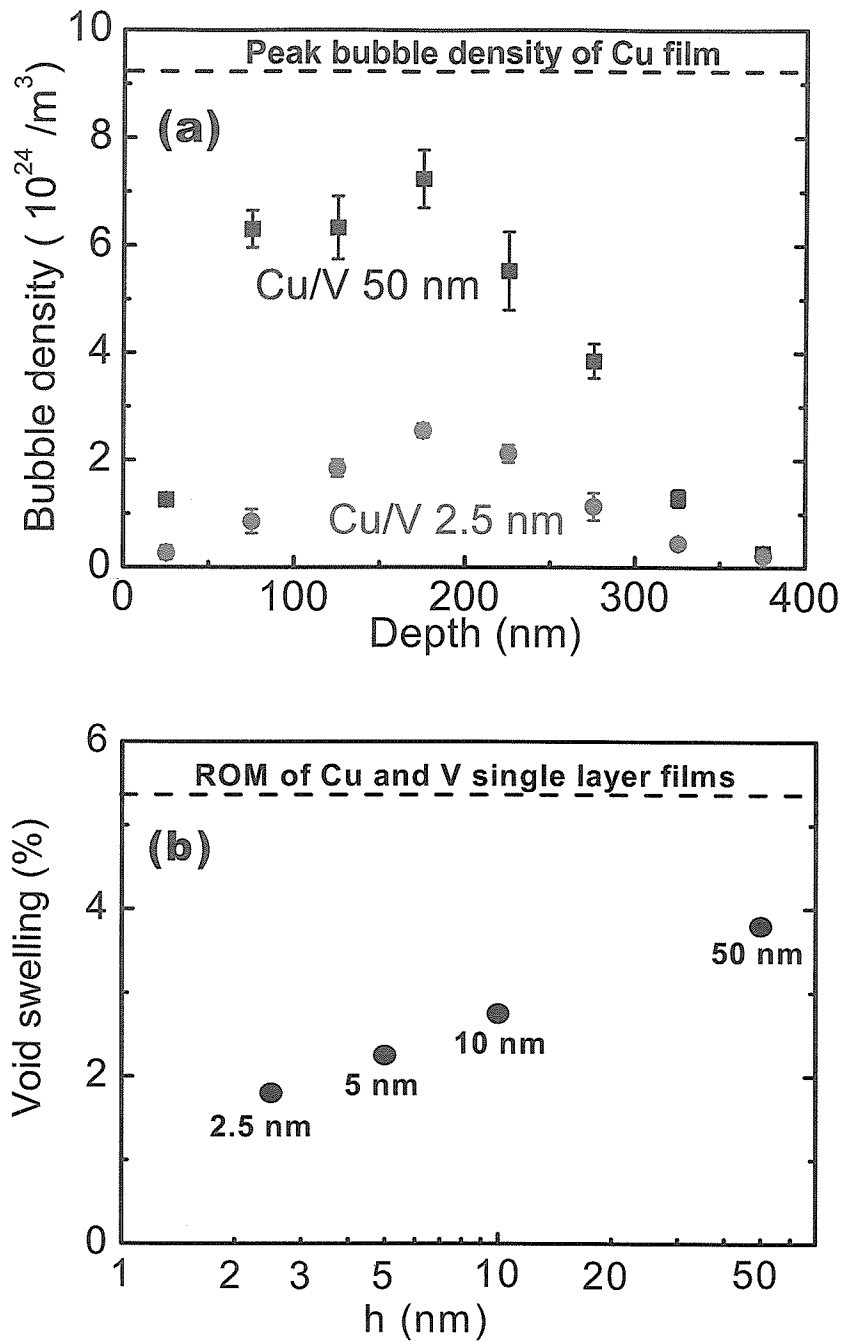


Figure 3, (a) Comparison of helium bubble density profiles from the surface in ion irradiated Cu/V 50 nm and Cu/V 2.5 nm nanolayers, and (b) void swelling vs.  $h$  in ion-irradiated Cu/V nanolayers, where  $h$  is individual layer thickness. The rule-of-mixture (ROM) void swelling in irradiated Cu and V single layer films is also shown by the horizontal dashed line.

To provide a rough estimate of radiation-induced void swelling, the step height across the irradiated and unirradiated (no radiation) region was measured by a profilometer and the results are shown in Fig. 3b. The magnitude of void swelling clearly decreases with decreasing  $h$ . The void swelling in irradiated Cu/V 2.5 nm nanolayer is approximately 2 times lower than that in Cu/V 50 nm nanolayers. Furthermore, void swelling in all irradiated Cu/V nanolayers is less than rule-of-mixture (ROM) void swelling in irradiated single layer Cu and V films, shown by the horizontal dashed line in Fig. 3b. An average of the measured void swelling in single layer Cu and V films subjected to identical irradiation conditions as the nanolayers was used as a reference and referred as ROM void swelling.

### 3.2 Irradiation induced hardening

Hardnesses of as-deposited and ion-irradiated Cu/V nanolayers vs  $h^{-0.5}$  are plotted in Fig. 4a, where  $h$  is the individual layer thickness. When  $h$  is greater than  $\sim 25$  nm, the hardness of as-deposited Cu/V scales approximately linearly with  $h^{-0.5}$ . The hardness approaches peak values at  $h$  of 2.5 nm or less. The ion irradiation in general leads to the increase of film hardness (radiation hardening). But the magnitude of radiation hardening diminishes continuously with decreasing  $h$ , and become negligible at  $h \leq 2.5$  nm. ROM hardness values of as-deposited and ion-irradiated films are also shown by the horizontal dashed lines in the same plot, respectively, with an ROM hardness increase of  $\sim 1$  GPa after irradiation. In order to examine hardness variation in more detail, the change of hardness between the as-deposited and ion-irradiated Cu/V specimens,  $\Delta H$ , as a function of  $h^{-0.5}$ , was plotted in Fig. 4b. The magnitude of  $\Delta H$  (indicated by black triangle) increases with increasing  $h$  and approaches the values of radiation hardening in single layer Cu and V films.

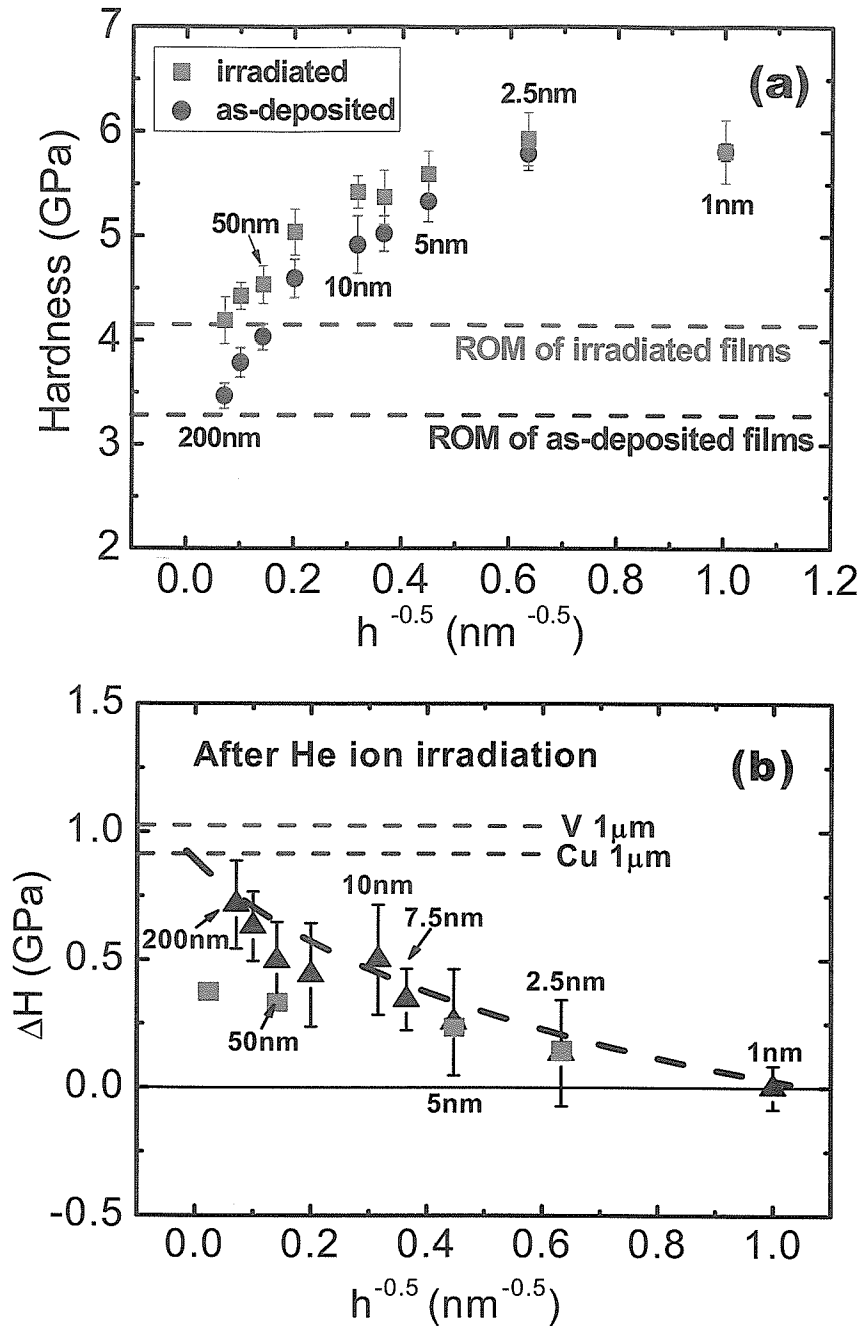


Figure 4, (a) Comparison of hardnesses of the as-deposited and irradiated Cu/V nanolayers as a function of  $h^{-0.5}$ . Rule-of-mixture (ROM) hardness values of as-deposited and ion-irradiated films are also shown by the horizontal dashed lines, respectively. (b) A plot of hardness variation of Cu/V nanolayer films as a function of  $h^{-0.5}$ . The magnitude of radiation hardening (indicated by black triangles) clearly increases with increasing  $h$ , and it is negligible when  $h$  is 2.5 nm or less. Red squares show the calculated He bubble induced hardening based on the FKH model.

## 4. Discussion

In this section, the evolution of microstructures, including the retention of layered morphology and generation of He bubbles is first examined and then the implication of these microstructural changes on irradiation hardening is analyzed.

### 4.1 Morphological stability of Cu/V layer interfaces

An energetic ion beam can induce ion mixing at interfaces between dissimilar materials. Such energetic ion induced ballistic mixing can effectively induce the formation of new phases or even completely destruct layer interfaces in miscible systems, such as Cu/Au [16]. However, in Cu/V system with a positive heat of mixing,  $\sim 5$  kJ/mol [54], a chemically driven demixing process may have occurred simultaneously during irradiation experiments. Hence the strong demixing tendency led to the retention of Cu/V layer interfaces. Similar phenomena have been observed in several other immiscible systems, such as Cu/W [16]. The mutual solid solubility between Cu and V is very limited, approximately 2.5 wt. % Cu in V matrix at 800 °C [17]. Intermixing at the level of a few at. % is below the detection limit of the STEM technique used in this study.

### 4.2 Radiation induced He bubbles

We now attempt to analyze radiation induced defect concentration in nanolayers. The primary radiation damage event in crystalline metals is the displacement of one or more atoms, and consequently vacancies, self-interstitials and foreign elements are created in crystal lattices [18]. In bulk FCC metal with low-to-medium stacking fault energy (SFE), such as Cu ( $\gamma_{SF} = 39$  mJ/m<sup>2</sup>) [19], approximately 90% of neutron radiation-induced defects are stacking fault tetrahedral (SFT) at a density of  $2-6 \times 10^{23}$  /m<sup>3</sup> at a

damage level of 0.01 - 0.9 dpa [20]. In BCC bulk V, radiation induced defects are mostly dominated by interstitial loops, 2 nm in diameter, at a density level of  $1-2 \times 10^{23}/\text{m}^3$  [20]. He will rapidly combine with vacancies and vacancy clusters to form bubbles.

He bubbles have been observed in most irradiated Cu/V nanolayers. The size and density are crucial to depict the He bubbles. The average bubble size at in-focus condition, determined based on a series of XTEM images (not shown here) by the intercept of linear fit with  $y$  axis, is  $0.7 \pm 0.2$  nm, and  $0.6 \pm 0.2$  nm in irradiated Cu/V 50 nm, and Cu/V 2.5 nm specimens, respectively. Such analysis indicates that the average bubble size depends very little on  $h$  of the nanolayers, and provides the basis for accurate determination of He bubble density. The reduction of He bubble density in Cu/V 2.5 nm specimen by a factor of approximately 3 compared to that in irradiated Cu/V 50 nm and Cu films indicates that vacancy concentration must have been dramatically reduced.

The equilibrium distribution function of He bubbles with the number of vacancies,  $n$ , and gas atoms,  $x$ , can be expressed by [4]

$$\rho^0(n, x) = M_x \exp\left\{n \ln S_v - \xi n^{2/3} + x \ln\left(\frac{MHn\Omega}{xkT}\right)\right\} \quad (1)$$

Where  $M_x$  is the number of gas-atom clusters per unit volume composed of  $x$  gas atoms,  $S_v$  is the supersaturation of vacancies,  $\xi$  is a temperature dependent constant,  $M$  is the overall He concentration in metals,  $H$  is the Henry's law constant for the dissolution of He in the metal,  $\Omega$  is the atomic volume of metals.  $S_v$  can be expressed by

$$S_V = \frac{C_V}{C_{V_0}} \quad (2)$$

Where  $C_V$  and  $C_{V_0}$  is the vacancy concentration and thermal equilibrium vacancy concentration, respectively.  $\xi$  can be written as

$$\xi = (36\pi\Omega^2)^{1/3} \frac{\gamma}{kT} \quad (3)$$

Where  $\gamma$  is the surface energy of solid.

Inspection of equation (1) shows that for Cu/V 2.5 nm and Cu/V 50 nm nanolayers, the major difference in the two systems is the first term in the bracket,  $S_V$ . Hence, assuming the thermal equilibrium vacancy concentration is similar in both systems, the reduced He bubble density at smaller layer thickness should be a direct evidence of reduced vacancy concentration,  $C_V$ , in nanolayers, via annihilation with interstitials.

It is generally accepted that radiation induced defects tend to migrate to the interfacial regions, such as grain boundaries and interfaces [21]. These interfacial regions are expected to act as effective sinks for radiation induced defects. The interfacial area density of defect sinks (number of interface per unit length along a direction normal to the layer interfaces) in Cu/V 2.5 nm nanolayers is 20 times higher than that in Cu/V 50 nm nanolayers. It is likely that defect migration along interface is facilitated, an event that leads to enhanced annihilation of opposite type defects. Mathematically, the reduced supersaturation of vacancies could also be affected by  $C_{V_0}$  to a certain extent, which is dependent on temperature and vacancy formation energy in thermal equilibrium state.

Recent MD simulation studies of Cu/Nb nanolayer films showed the formation energies of vacancies are significantly lower at Cu/Nb interfaces than in the perfect crystals of the neighboring elements [22]. Hence it is likely that when  $h$  in the nanolayer is reduced to a few nm length scale, the value of  $C_{V_0}$  is slightly increased due to the interface effect. As a result the capacity of defect storage in nanolayer is enhanced and reduces the supersaturation of vacancies. The reduction of He bubble density in nanolayers is thus a combined effect of enhanced defect storage capacity (increasing  $C_{V_0}$ ) and increased probability of defect annihilation at interfaces (decreasing  $C_V$ ).

#### **4.3 Mechanical integrity and hardening mechanisms**

In conventional metals, radiation hardening is contributed by interaction of dislocations with two types of radiation-induced defects: strong obstacles, such as interstitial loops, SFTs and precipitates, and relatively weak obstacles, such as He bubbles [23]. The interaction of glide dislocations with Cu/V interfaces is not expected to change significantly given the retention of chemically abrupt interfaces after radiation. As noted in previous reviews of obstacle-controlled strengthening, the dispersed barrier model [24] is appropriate for strong obstacles induced hardening. An alternative hardening relationship was developed by Friedel-Kroupa-Hirsch (FKH) for weak obstacles [25, 26]. The contribution of He bubbles to radiation hardening is negligible at low He concentration and becomes significant only above a critical He concentration around 1 at. % [27-29]. The SRIM simulation results predict the average He concentration is around 1.9 at. % in Cu/V 50 nm nanolayers and 1.6 at. % in Cu/V 5 nm nanolayers, respectively. When the bubble size is very small, He bubbles are treated as

the weak obstacle. The FKH model is applied to estimate the He bubbles induced enhancement of yield strength,  $\Delta\sigma$ , by:

$$\Delta\sigma = \alpha M \mu b d N^{\frac{2}{3}} \quad (4)$$

Where  $\alpha$  is typically taken as  $\sim 1/8$  [30].  $M$  is the Taylor factor taken as 3.06 for FCC and BCC metals, and  $\mu$  is the shear modulus of 46 GPa for both Cu and V;  $b$  is the Burgers vector of the primary glide dislocations. The magnitude of Burgers vector in FCC Cu is  $a_{Cu}/\sqrt{2} = 0.3615/\sqrt{2} = 0.25562$  nm and in BCC V is  $a_V\sqrt{3}/2 = 0.3027 \times \sqrt{3}/2 = 0.26218$  nm, respectively. The diameter of He bubbles ( $d$ ),  $\sim 1$  nm, and their average number density ( $N$ ) across the radiation damage region are obtained from TEM measurements. Radiation hardening, estimated as three times of the calculated  $\Delta\sigma$  indicated by red squares, is compared with experimental values (indicated by black triangles) in Fig. 4b. It is evident that insignificant radiation hardening in nanolayers at smaller  $h$  (a few nm or less) can be described well by He bubble induced hardening. However, He bubble induced hardening alone underestimates the experimental values for single layer Cu film, single layer V film and that of nanolayers with greater  $h$  (50 nm for instance). The above analyses show that the magnitudes of radiation hardening due to He bubbles are less than experimental measurement, implying radiation hardening contributions from other factors, presumably interstitial loops.

We noticed that, in spite of a rather high He bubble density, the average distance between He bubbles ( $\lambda$ ) is  $\sim 25$  nm, a length scale where Orowan type of dislocation bowing between bubbles is a reasonable mechanism. Depending on the difference

between inter bubble separation ( $\lambda$ ) and the individual layer thickness,  $h$ , radiation hardening in nanolayers could be categorized into three regimes. (i) For  $h \ll \lambda$ , at a few nm length scale, the yield strength of the nanolayers is expected to be controlled by the smaller length scale,  $h$ , with minimal contribution from He bubbles. (ii) When  $h$  is comparable to  $\lambda$ , radiation hardening from bubbles will become more evident. (iii) Finally when  $h$  is much greater than  $\lambda$ , on the order of hundreds of nm, the magnitude of radiation hardening approaches that of single layer films, and significant hardening by irradiation-induced defects is expected. In addition to He bubbles, other defects, such as interstitial loops will also become important. At small  $h$ , interstitials are expected to migrate to interface sinks and hence, loops may not form within layers.

The interstitial loops are typically treated as the strong barriers to the trespassing of the dislocations in the radiation studies. The dispersed barrier model based on straightforward geometrical considerations for obstacles intersecting the dislocation slide plane is the most appropriate for strong obstacles such as interstitial type dislocation loops. So the yield strength for polycrystalline metal is predicted by the well-known dispersed barrier hardening equation:

$$\Delta\sigma = M\alpha'\mu b\sqrt{Nd} \quad (5)$$

Where  $M$ ,  $\mu$ ,  $b$ ,  $N$  and  $d$  carry the same physical meanings as defined previously, but this time the defect clusters are interstitial loops.  $\alpha'$  is a parameter that depends on the average barrier strength of the radiation-induced defect clusters. Recent studies estimate  $\alpha$  is 0.26 for V and 0.2 for Cu [20]. By subtracting the contribution of He bubble induced hardening from measured values, the average interstitial loop density

with an assumption of size of 2 nm is estimated as  $0.5 \times 10^{23} / \text{m}^3$  for Cu/V 50 nm nanolayer. This is comparable to the interstitial loop density of  $6.7 \times 10^{23} / \text{m}^3$  and  $2.3 \times 10^{23} / \text{m}^3$  in neutron-irradiated polycrystalline pure Cu and V metals subjected to a total dose of 0.92 dpa and 0.69 dpa, respectively [20].

Finally we noticed that the underestimation of radiation hardening by He bubbles alone could also be attributed to the use of a constant  $\alpha$  value of 1/8 in eq. 4. Our analysis shows that an  $\alpha$  value varying from 1/8 (for Cu/V with smaller  $h$ ) to  $\sim 1/3$  (single layer Cu or V) can fit the experimental results of radiation hardening well. A higher  $\alpha$  value would indicate a greater number of helium atoms per bubble or higher pressure inside bubbles. At higher  $h$ , less interface area is available to trap He. So a higher concentration of helium may be trapped in the bubbles within the layers, making bubbles stronger barriers for the glide of dislocations. To elucidate this hypothesis future studies are needed to probe the pressure in bubbles in nanolayers of different  $h$ .

#### **4.4 The significance of Cu/V interface in enhancing radiation resistance in nanolayers**

Our study clearly demonstrates that in the nearly immiscible Cu/V system, layer interfaces play significant roles in enhancing radiation resistance of the nanolayers, manifested as reduced He bubble density and less radiation hardening. The fundamental mechanisms of interface-driven enhancement of radiation tolerance can be interpreted as follows.

(1) Interfaces (between Cu and V) act as sinks for defects (vacancies, interstitials and helium atoms), since defect formation energy is lower at interfaces than in crystal lattices [22]. Furthermore MD simulations of Cu/Nb interface show that misfit dislocations

evolve into extended jog pairs and significantly increase the sink capacity of Cu/Nb interfaces [13]. Since the immiscible Cu/V has similar interface (fcc/bcc type with K-S orientation relationship) comparing to immiscible Cu/Nb, we anticipate that the Cu/V interface will also have high sink capacity for point defects.

(2) Interfaces promote annihilation of unlike defects as defects have high mobility and delocalized cores [13] at interfaces. Our recent MD simulation studies [13, 22] have shown that interfaces will athermally absorb and annihilate point defect within 2ps after their generation up to a distance of approximately 1-2 nm from the interface. With an interface spacing of 2.5 nm in Cu/V 2.5nm nanolayers, the distance between cascade events and interfaces is expected to be small enough to allow direct interaction without the need for diffusion. So the annihilation process in these very fine nanolayers should occur almost instantaneously with the collision cascades. Whereas in bulk lattices (Cu/V 100 nm instance), the interface-defect interactions will depends on both the length and time scales.

(3) Interfaces also have a high solubility for helium, and hence, such an effect combined with reduced vacancy concentration due to enhanced annihilation defers the bubble nucleation to higher helium concentration.

(4) Interfaces in Cu/V nanolayers can significantly reduce the densities of defect clusters such as interstitial loops, stacking fault tetrahedra, and more importantly He bubbles, and hence, dramatically alleviate void swelling and suppress irradiation hardening. Furthermore the significance of interface is also manifested from a clear size (layer thickness) dependent reduction of void swelling and irradiation hardening.

## Summary and conclusions

The evolution of microstructure and mechanical properties of sputtered Cu/V nanolayers subjected to 50 keV He ion irradiation were investigated systematically. Irradiated nanolayer interfaces remain chemically abrupt even in the peak damage region upon a total dosage of  $\sim 6$  dpa. Such immiscible layer interface can effectively reduce the overall concentration of He bubbles, interstitial loops and void swelling, the magnitude of which reduces at smaller individual layer thickness. These nanolayers also show clearly a monotonic suppression of radiation hardening at smaller layer thickness due to the effective attraction and facilitated annihilation of Frenkel pairs. Nanolayers with immiscible layer interface hence offer a promising approach in alleviating void swelling and radiation hardening.

## Acknowledgements

The author acknowledges financial support by DOE-NERI, Office of Nuclear Energy, Science and Technology, AFCI program, under grant number DE-FC07-05ID14657. Usage of ion accelerator in Accelerator Laboratory, directed by Dr. L. Shao, at Texas A&M University is also acknowledged.

## References

- [1] T. Leguey, N. Baluc, R. Schäublin and M. Victoria, *J Nucl Mater* 307 (2002) 696.
- [2] F. A. Garner, M.B. Toloczko and B.H. Sencer, *J Nuclear Mater* 276 (2000) 123.
- [3] H. Trinkaus and B.N. Singh, *J Nucl Mater* 323 (2003) 229.
- [4] G. Was, *Fundamentals of radiation materials science*, Springer, New York, 2007.

- [5] F.A. Garner, B. Oliver, L.R. Greenwood, M.R. James, P.D. Ferguson, S.A. Maloy and W.F. Sommer, *J Nucl Mater* 296 (2001) 66.
- [6] D.L. Porter and F.A. Garner, *J Nucl Mater* 159 (1988) 114.
- [7] N. Hashimoto, T.S. Byun and K. Farrell, *J Nucl Mater* 351 (2006) 295.
- [8] K. Shiraishi, K. Fukaya and Y. Katano, *J Nucl Mater* 54 (1974) 75.
- [9] T.S. Byun and K. Farrell, *J Nucl Mater* 326 (2004) 86.
- [10] M. Rose, A.G. Balogh and H. Hahn, *Nucl. Meth. Phys. Res. B*, 127 (1997) 119.
- [11] M. T. Robinson, *J Nucl Mater* 216 (1994) 1.
- [12] T. Hochbauer, A. Misra, K. Hattar and R.G. Hoagland, *J Appl Phys* 98 (2005) 123516.
- [13] M.J. Demkowicz, R.G. Hoagland and J.P. Hirth, *Phys Rev Lett* 100 (2008) 136102.
- [14] E.G. Fu, Nan Li, A. Misra, R. Hoagland, H. Wang, and X. Zhang, *Mater Sci Eng A* 493 (2008) 283.
- [15] J.F. Ziegler, M.D. Ziegler and J.P. Biersack, (<http://www.srim.org/>).
- [16] H. Westendorp, Z-L. Wang and F.W. Saris, *Nucl Instrum Meth* 194 (1982) 543.
- [17] T.B. Massalski, J.L. Murray, L.H. Bennett and H. Baker, *Binary Alloy Phase Diagrams*, American Society for Metals, Metals Park, Ohio, 1986.
- [18] H. Trinkaus, *J Nucl Mater* 318 (2003) 234.
- [19] R. Schäublin, Z. Yao, N. Baluc and M. Victoria, *Philos Mag* 85 (2005) 769.
- [20] N. Hashimoto, T. S. Byun, K. Farrell and S. J. Zinkle, *J Nucl Mater* 329 (2004) 947.
- [21] S. M. Bruemmer and G. S. Was, *J Nucl Mater* 216 (1994) 348.
- [22] A. Misra, M.J. Demkowicz, X. Zhang and R.G. Hoagland, *JOM*, 59 (2007) 62.
- [23] G.E. Lucas, *J Nucl Mater* 206 (1993) 287.

- [24] A.K. Seeger, in: Second UN Conference on Peaceful Uses of Atomic Energy, vol.6 United Nations, New York, 1958, p.250.
- [25] J. Friedel, Dislocations, Pergamon, New York, 1964.
- [26] F. Kroupa, P.B. Hirsch, Disc Faraday Soc 38 (1964) 49.
- [27] H. Ullmaier, E. Camus, J Nucl Mater 251 (1997) 100.
- [28] J.D. Hunn, E.H. Lee, T.S. Byun, L.K. Mansur, J Nucl Mater 282 (2000) 131.
- [29] E.H. Lee, T.S. Byun, J.D. Hunn, K. Farrell, L.K. Mansur, J Nucl Mater 296 (2001) 183.
- [30] S.J. Zinkle and Y. Matsukawa , J Nucl Mater 329-333 (2004) 88.